Available online at www.eccomasproceedia.org
Eccomas Proceedia COMPDYN (2025) 5109-5121

ECCOMAS
Proceedia

COMPDYN 2025
10th ECCOMAS Thematic Conference on
Computational Methods in Structural Dynamics and Earthquake Engineering
M. Papadrakakis, M. Fragiadakis (eds.)
Rhodes Island, Greece, 15-18 June 2025

THE EFFECTS OF MOISTURE-INDUCED DEGRADATION ON THE STRUCTURAL PERFORMANCE OF HISTORICAL BUILDINGS: A CASE STUDY

Matteo Sticchi[1], Gianni Blasi[1], Emilia Vasanelli[2] and Maria A. Aiello[1]

[1] Department of Engineering for Innovation
University of Salento
Piazzetta Tancredi 7, 73100 Lecce, Italy
{matteo.sticchi, gianni.blasi, antonietta.aiello}@unisalento.it

[2] Institute of Heritage Science
National Research Council
Via per Monteroni, 73100 Lecce, Italy
emilia.vasanelli@cnr.it

Abstract

A significant fraction of Italian building scenario consists of historic masonry buildings with high cultural value. In recent years, structural health assessment and monitoring of such buildings has become fundamental, not only for heritage conservation matters, but also for safety. In fact, several historical buildings are used for strategic assets (e.g. administration offices, police stations, education services). Therefore, assessing the seismic vulnerability of these structures, along with the effects of material degradation over time, is crucial to ensure their preservation. Literature studies and recent tragic events evidenced the urgency of retrofitting highly degraded historical structures, to prevent major consequences on society. To this regard, the accurate assessment of the structural performance degradation due to material ageing is an aspect of paramount importance. In the case of masonry structures, moisture content reduces the compressive strength and Young's modulus of stone materials.
This study analyses the effects of moisture-induced degradation on a case study strategic masonry building, realized using Lecce Stone walls typical of southern Apulian regions. In-situ investigation alongside literature results were used to define mechanical properties of bricks at different saturation levels, aiming to develop degradation-dependent constitutive laws.
Subsequently, a finite element model of the case study building was developed, aiming to investigate the evolution of structural performance over time depending on the moisture-induced material degradation. Modelling uncertainties were considered to define a worst-case and a best-case degradation scenario. Linear time-history analyses using spectrum-compatible ground motions were performed to evaluate the impact of moisture on the dynamic properties and floor response spectra.

Keywords: Masonry structures, Structural performance degradation, Floor response spectra, Seismic vulnerability.

ISSN:2623-3347 © 2025 The Authors. Published by Eccomas Proceedia.
Peer-review under responsibility of the organizing committee of COMPDYN 2025.
doi: 10.7712/120125.12798.25841

1 INTRODUCTION

A significant fraction of the Italian building scenario is characterized of masonry structures. Aging and lack of maintenance contribute to material degradation, increasing structural vulnerability. Consequently, major seismic risk is associated with such structures in high seismic hazard zones (e.g. Italy). Collapses of masonry structures caused by recent earthquakes in Italy drawn the attention of public administrations to structural health monitoring and performance evolution prediction. Beyond heritage preservation, many of these buildings serve strategic functions (e.g., administrative offices, police stations, educational facilities), evidencing the need of seismic vulnerability assessment for risk mitigation and public safety.

In this scenario, long-term material deterioration is a key aspect affecting global structural performance and local failures over time, which should be accurately considered to schedule maintenance and retrofit interventions.

Among the main causes of degradation in masonry structures, moisture plays a crucial role, as it alters mechanical properties and contributes to long-term performance loss [1, 2]. According to ICOMOS definitions [3, 4], degradation refers to the loss of material quality and functionality over time. Specifically, the presence of water can lead to surface erosion, contaminant deposition, salt crystallization, and biological growth. All these factors contribute to accelerated deterioration, especially in porous materials.

Past studies showed that moisture significantly reduces the compressive strength and elastic modulus of stones commonly used for construction. Laboratory tests were performed on masonry panels or bricks, which were conditioned to achieve different moisture through direct water immersion or exposure to controlled humidity environment [5]. Uniaxial compression tests performed after the conditioning period consistently reported strength degradation as saturation level increases. Different types of stones were analysed, namely tuff stones [6, 7], calcarenites [8, 9], sandstones [10], clay stones [11, 12].

In this study, a comprehensive review of the literature studies on moisture-induced mechanical performance degradation of masonry walls is carried out. The collected data were used to develop a simplified relationship between saturation level and compressive strength decay, depending on the type of stone considered. An average compressive strength reduction of $42.99 \pm 21.20\%$ was detected, based on 264 tests. The obtained data-driven relationship was used to evaluate structural performance decay of a case study masonry building, depending on saturation level of masonry. The case study is a public building made of Lecce stone, a typical calcarenite of the Apulia region. Due to limited experimental data available on this material, in-situ investigations were conducted to estimate mechanical properties of masonry and perform a correlation with similar materials examined in the literature. Subsequently, linear time-history analysis of the building was conducted assuming four different saturation scenarios of the walls, where mechanical decay was addressed by reducing the equivalent elastic modulus of the masonry based on the data-driven relationship obtained from the literature review. A set of spectrum compatible ground motions at damage limitation (DL) performance level were considered for the time history analysis, selected according to Italian seismic design code [13]. The results of the analyses were used to compute floor response spectra for each scenario considered, aiming to evaluate the variation of the seismic response of the building depending on the moisture content.

2 DESCRIPTION OF THE CASE STUDY

The selected case study is the “Buon Pastore” building, a historic masonry structure located in Lecce (Apulia, Italy), currently undergoing structural and energy retrofitting. The building

was subject to several structural modifications over its service life, including retrofit with reinforced concrete (RC) frames inclusion.

An on-site testing campaign was carried out to assess material properties and degradation phenomena. The structural system construction technique is homogeneous for almost all the building. The vertical elements are characterized by masonry walls with thickness ranging from 20 to 130 cm, composed of Lecce stone bricks and lime mortar joints. The floors are mainly realized through cross vaults, while RC slabs are present in a limited number of areas from the mezzanine level up to the roof, which were built during a later construction phase. The building exhibits extended moisture-related degradation phenomena due to rising damp and rainwater (Figure 1).

(a) (b) (c)

Figure 1: Moisture penetration in (a) vaults and (b) RC slab and (c) masonry walls.

2.1 On-site Investigations

The literature review highlighted a lack of specific data regarding the variation of Lecce stone's mechanical properties under different saturation levels. To address this gap, a non-destructive in-situ testing campaign was carried out on the case study building for mechanical characterization of construction materials.

Tomographic and ultrasonic pulse velocity (UPV) tests were performed using a PROCEQ Pundit PD8050 device with 24 transducers. This instrument provides an initial estimate of wave propagation velocities measured between transducers on the surface, which are then calibrated on the brick thickness and the material properties, assuming a Poisson's ratio of 0.2 [14]. The calibrated surface velocity measurements are summarized in Table 1.

Measurement	UPV_TOM [*m/s*]
T1	2260.88
T2	2132.69
T3	2501.75
T4	2616.87
T5	3006.34

Table 1: In-situ tomographic measurements.

The results were used to estimate compressive strength and elastic modulus through literature-based correlations [15]. The obtained values of compressive strength were used to calibrate mechanical models adopted in the numerical simulation described in the following.

3 STATISTICAL ANALYSIS OF MOISTURE-INDUCED DEGRADATION OF MECHANICAL PERFORMANCE

The mechanical properties of the masonry were defined by combining on-site test results with literature-based degradation data, aiming to estimate compressive strength and elastic modulus decay as function of the saturation level. Aiming to address material degradation effect in the numerical study, a dataset on mechanical performance of masonry wall specimens subjected to water saturation conditioning was developed, based on a literature review of laboratory tests. The results included in the dataset were carried out on different stone materials, including tuff stones, sandstones, limestones and clay stones.

All the studies consisted of uniaxial compression tests on dry and fully saturated specimens, aiming to evaluate the compressive strength decay based on saturation. The results were grouped in five categories, differing in material type. The average compressive strength decay with respect to the dry state, Δf_c, and relative standard deviations, σ, are reported in Table 2 and Figure 2.

Material Type	Δf_c [%]	σ [%]
Clays	16.20	5.53
Tuffs	50.81	21.14
Sandstones	37.28	22.69
Limestones	39.65	18.76
Others	35.62	10.36

Table 2: Average compressive strength decay from dry to fully saturated state obtained for each stone type.

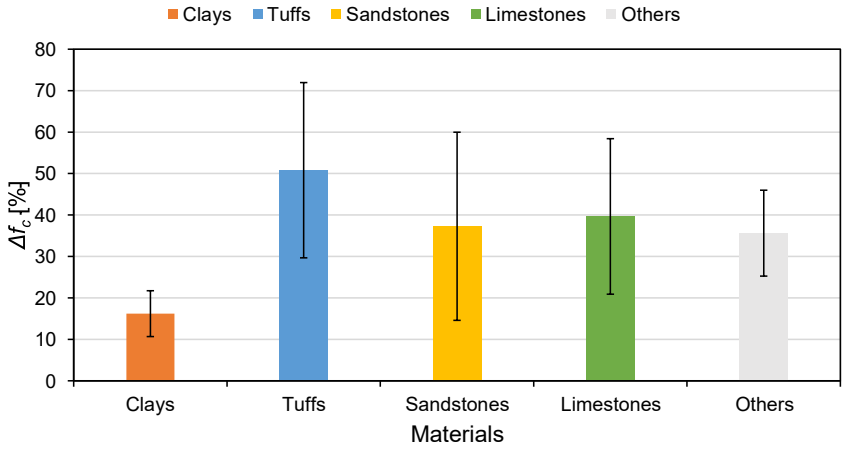

Figure 2: Average compressive strength reduction at complete saturation (%) for different materials with standard deviation.

Tuff stone specimens showed both the highest Δf_c (50.8%) and variability (CoV = 0.42). Limestones and sandstones specimens feature similar values of Δf_c (39.7% and 37.3%, respectively). Clay stone specimens exhibited the lowest Δf_c (<20%), while other materials showed intermediate behaviour (~35%). The observed results reveal a strong correlation between material type and degradation level. In fact, more porous and weakly cemented stones had greater strength loss under saturation conditions. The associated data dispersion is consistent with the

variability in petrographic composition and material porosity, as well as with the different testing standards adopted in the studies.

Referring to calcarenite stones, representative of the case study material (Lecce stone), the ratio between conditioned and dry strength, α, was computed for each test collected. The average value obtained for α is equal to 0.6, with a standard deviation of 0.18. Aiming to account for the uncertainties in defining mechanical performance decay, the 15th and 85th percentiles (P_{15} and P_{85}, respectively) were also computed (equal to 0.38 and 0.85, respectively).

Hence, the values of P_{15} and P_{85} were used to define two additional strength degradation scenarios under fully saturated conditions for the masonry material of case study. Figure 3 illustrates the relationship between the saturation level and the compressive strength of limestone elements within the P_{15}-P_{85} range. Additionally, single data referred to each considered test are reported.

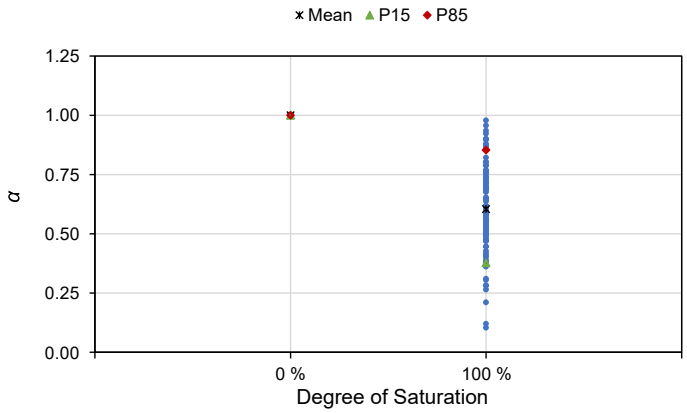

Figure 3: Literature-based Degradation model for limestones.

4 NUMERICAL MODEL

An elastic numerical model of the case study was developed in STKO [16], aimed at evaluating the effect of moisture-induced material degradation on the dynamic response of the building. The numerical model is depicted in Figure 4.

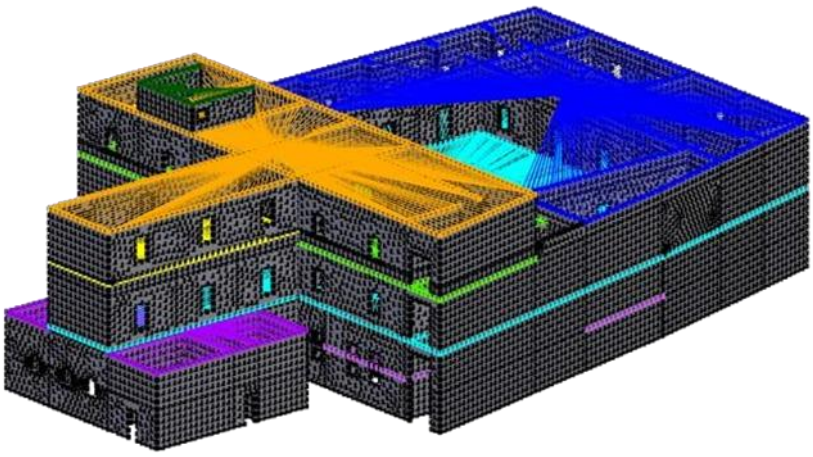

Figure 4: Numerical model of the case-study structure.

Triangular layered shell elements were used to model masonry walls, allowing a simulation of both in-plane and out-of-plane behaviour. The vaults and the RC slabs were not explicitly defined in the numerical model, and their contribution to lateral stiffness was considered by including rigid diaphragm constraints at each floor level. Soil-structure interaction was neglected, due to the low intensity of the seismic action considered. The connection to the foundation elements was modelled by restraining in-plane displacements of the base nodes of the system.

Due to the complexity of the geometry and, consequently, to the high computational efforts, the mass of each floor was lumped at its centre of mass, by including a fictitious node with associated horizontal translational mass and rotational mass around the vertical axis.

A homogeneous equivalent material was assigned to the shell elements, whose mechanical properties were derived from those of bricks and mortar. The mechanical properties of Lecce Stone bricks were defined based on in-situ tests. Particularly, UPV measurements obtained from tomographic testing were correlated to uniaxial compressive strength (UCS) using the Equation (1) proposed by Vasanelli et al. [15].

$$UCS = 0.0159 \cdot UPV - 27 \quad (1)$$

Subsequently, material properties under saturated conditions were computed, based on the results obtained from the collected dataset. In order to consider uncertainties in defining the mechanical decay, three degraded scenarios were defined, referred to the P_{15}, the average and the P_{85} value of α.

The computed values of UCS were combined with a class M2.5 mortar according to the Italian Standard [13] to obtain the equivalent masonry strength, f_m and elastic modulus, E. Particularly, the value of E was computed as $1000 \cdot f_m$. Concluding, four structural configurations were considered, referred to the dry state (Dry) and three saturated-states (Sat_15, Sat_mean, Sat_85), corresponding to the P_{15}, the average, and the P_{85} of the α distribution.

Table 3 shows a summary of the results. The value of α, the compressive strength of the block, f_b, the equivalent compressive strength of the masonry, f_m, and the equivalent Young's modulus, E, are provided.

Configuration	α	f_b [MPa]	f_m [MPa]	E [MPa]
Dry	1.00	8.61	3.77	3767.31
Sat_med	0.60	5.20	3.04	3039.58
Sat_15	0.37	3.24	2.12	2122.50
Sat_85	0.85	7.24	3.47	3468.89

Table 3: Mechanical properties of the bricks and the masonry obtained for each considered configuration.

5 MODAL PROPERTIES AND SEISMIC RESPONSE

5.1 Eigenvalue analysis

An eigenvalue analysis of the structure was conducted for each configuration considered. In Table 4, the main modal properties of the first three modes are provided, namely the mode directions, the modal periods, T, and the participating mass ratios, ρ.

As expected, longest periods were obtained for the case of Sat_15, characterized by the lowest value of compressive strength and, consequently, of elastic modulus. Referring to the

participating mass ratios, the same values were obtained for all the considered configurations, as stiffness and masses distribution of the structure is not affected by saturation level.

Configuration	Mode	Mass Contribution	ρ [%]	T [s]
Dry	1	M_Y	68.33	0.12539
	2	M_X	72.88	0.10513
	3	RM_Z	65.02	0.10079
Sat_15	1	M_Y	68.33	0.16706
	2	M_X	72.88	0.14006
	3	RM_Z	65.02	0.13429
Sat_Mean	1	M_Y	68.33	0.1396
	2	M_X	72.88	0.11704
	3	RM_Z	65.02	0.11221
Sat_85	1	M_Y	68.33	0.13067
	2	M_X	72.88	0.10956
	3	RM_Z	65.02	0.10504

Table 4: Summary of results from the Eigenvalue analyses of the four case study configurations.

5.2 Linear Time-History analysis

In order to assess the variability of the seismic response of the structure depending on the saturation level of masonry, a linear time history (LTH) analysis was conducted using STKO [16]. A set of 20 spectrum-compatible ground motion pairs (X and Y components) was selected for each structural configuration considered, according to the conditional mean spectrum approach proposed by Baker [17]. The target spectrum was defined assuming a return period of 75 years and soil type B, referring to the Italian seismic code provisions for use category III structures at DL performance level. The corresponding peak ground acceleration (PGA) for the site in Lecce was equal to 0.0264 g. Figure 5 shows the conditional spectra of the ground motions selected for each configuration, along with the design spectrum, the mean spectrum and the conditional mean spectrum within its deviation tolerance.

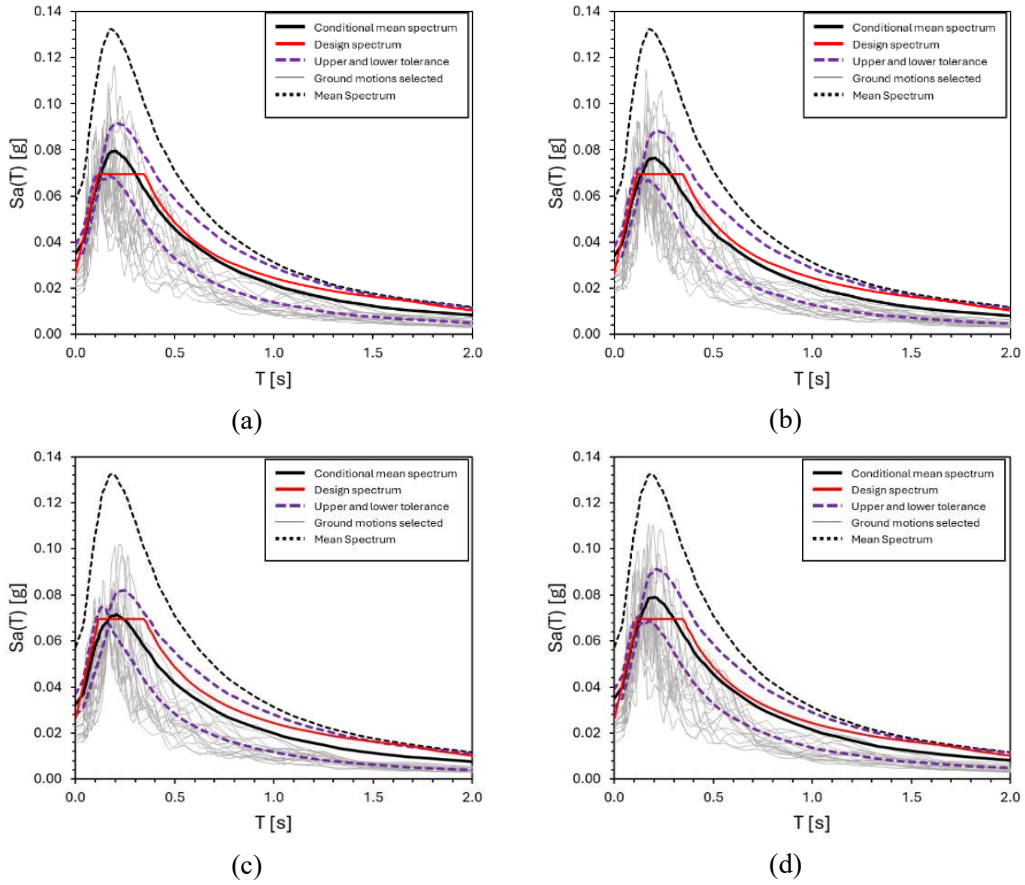

Figure 5: Conditional spectra of the selected ground motions for the configuration (a) Dry, (b) Sat_mean, (c) Sat_15 and (d) Sat_85.

5.3 Results and discussion

The results of the LTH analyses performed were examined in terms of acceleration and displacement time-history (TH) response at the centre of mass of each floor. Figure 6 shows the location of the centre of mass in both plan and elevation view.

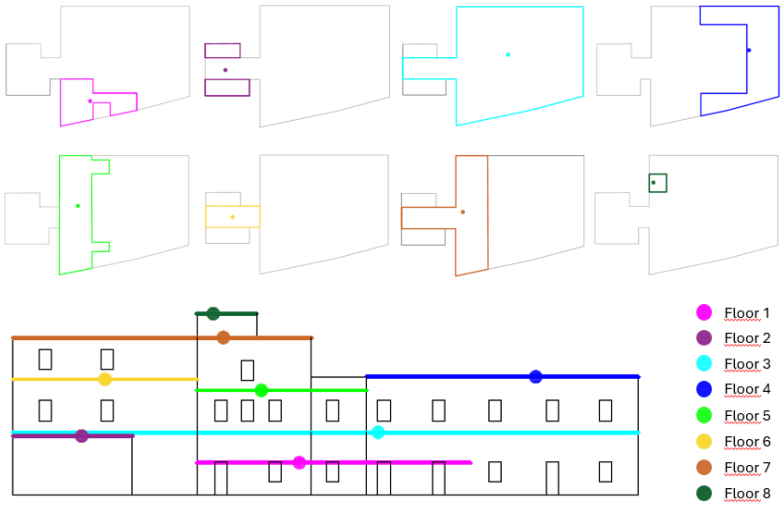

Figure 6: Location of centres of mass nodes in plan and elevation view.

As shown in Figure 6, eight nodes were selected along the height of the structure. Floors 1 to 3 correspond to the mezzanine, the roof of the chapel-side rooms and the first floor of the main system, respectively. Floors 4 to 8 refer to the roof of the front portion, the second floor, the roof of the rear portion and the roof of the elevator shaft, respectively.

The peak floor accelerations (PFAs) obtained at each level for all the considered configurations are provided in Figure 7, expressed as the SRSS of the X and Y component.

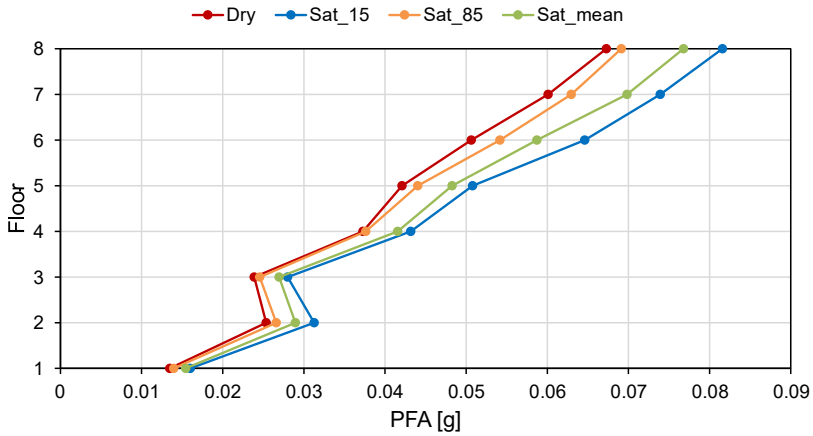

Figure 7: PFA profiles along building height for different saturation conditions.

The configuration with the lowest stiffness (Sat_15) consistently exhibited the highest PFAs, particularly at upper levels. Indeed, slightly higher spectral acceleration is observed in the conditional mean spectrum at the first period of Sat_15 (0.17 s), potentially resulting in higher PFAs. In contrast, the Dry configuration showed the lowest response, while Sat_mean and Sat_85 configurations exhibited intermediate behaviour. The Sat_85 configuration yielded PFAs close to the Dry configuration, consistently with their similar elastic moduli.

The average values, μ, of the PFAs obtained, alongside the standard deviation, σ, and the coefficient of variation, *CoV*, computed among the twenty ground motion inputs are provided in Table 5.

Configuration		Floors							
		1	2	3	4	5	6	7	8
Dry	μ	0.013	0.025	0.024	0.037	0.042	0.051	0.060	0.067
	σ	0.003	0.004	0.005	0.009	0.008	0.009	0.014	0.015
	CoV	0.186	0.157	0.201	0.250	0.199	0.186	0.229	0.217
Sat_15	μ	0.016	0.031	0.028	0.043	0.051	0.065	0.074	0.082
	σ	0.006	0.010	0.011	0.018	0.018	0.023	0.025	0.027
	CoV	0.349	0.325	0.377	0.410	0.356	0.350	0.341	0.326
Sat_85	μ	0.014	0.027	0.025	0.038	0.044	0.054	0.063	0.069
	σ	0.003	0.005	0.005	0.008	0.009	0.012	0.016	0.016
	CoV	0.202	0.194	0.196	0.224	0.199	0.213	0.249	0.232
Sat_mean	μ	0.015	0.029	0.027	0.042	0.048	0.059	0.070	0.077
	σ	0.004	0.006	0.006	0.012	0.012	0.014	0.021	0.023
	CoV	0.228	0.206	0.241	0.285	0.243	0.235	0.305	0.299

Table 5: Statistical summary of PFAs by floor and saturation condition.

Highest dispersion was observed for Sat_15, especially between Floors 3 and 5, where reduced stiffness increases sensitivity to record-to-record variability. In contrast, the Dry and Sat_85 configurations show lower *CoV*, while data from Sat_mean exhibited intermediate fashion. Overall, the results highlight that moisture both modifies PFAs and the variability of the seismic response under different ground motion inputs.

All configurations show an increase in acceleration with height, but the slope of this trend differs. The PFAs increase compared to the Dry configuration at the eight floor is approximately 3%, 14% and 21% for the Sat_85, Sat_mean and Sat_15 configurations, respectively. The Sat_15 profile shows a steep gradient, indicating a stronger amplification effect due to reduced stiffness. Conversely, the Dry and Sat_85 configurations show more gradual profiles. The eighth-to-first floor PFA ratio is approximately 5.1 for the Sat_15 configuration, while it is equal to 4.99, 4.97, and 4.95 for Dry, Sat_mean, and Sat_85, respectively.

The largest variation in PFA between the Dry and Sat_15 configurations is observed at the sixth floor. Furthermore, the highest dispersion in PFA values occurs at the fourth floor, with a *CoV* of 0.41.

To further investigate the influence of saturation on the seismic response, 5% damped floor response spectra (FRS) were computed at all floors in both principal directions. Figure 8 displays the average FRS obtained among the 20 input motions, computed as the square root of the sum of squares (SRSS) of the results along the two principal directions.

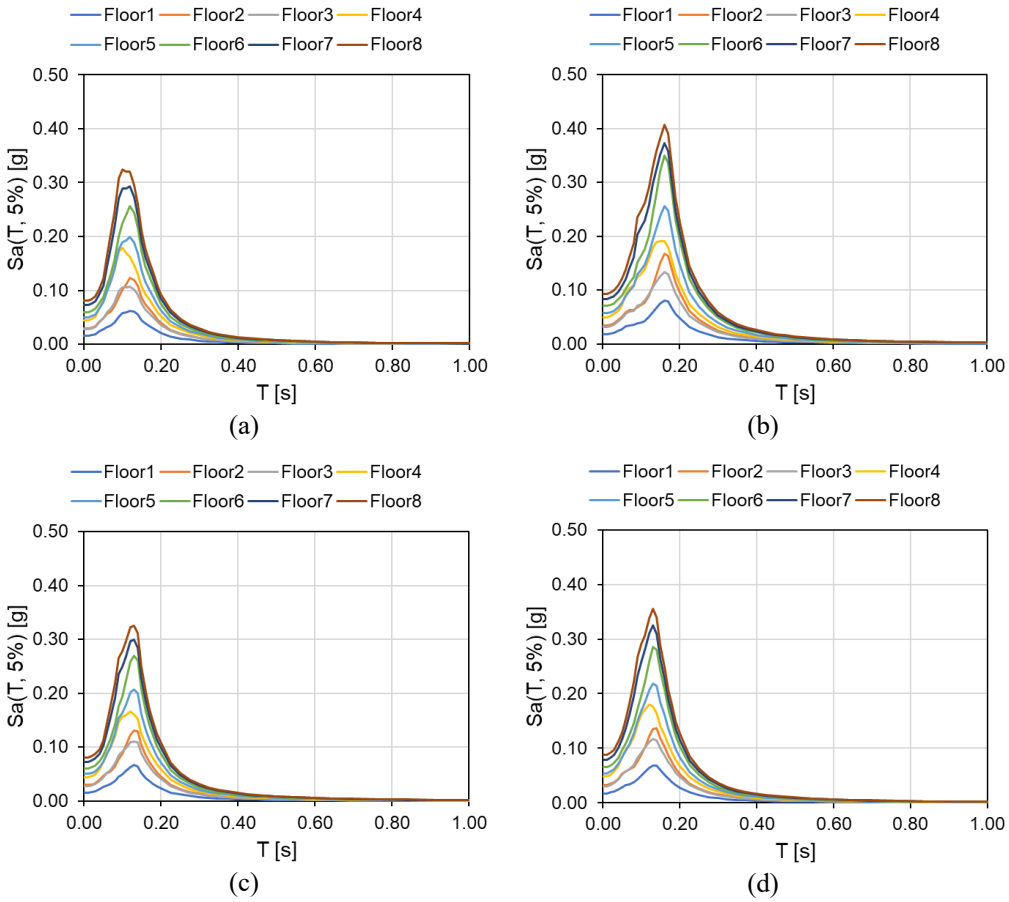

Figure 8: Mean floor spectra for the configuration (a) Dry, (b) Sat_15, (c) Sat_85 and (d) Sat_mean.

As expected, response amplification range is shifted towards higher values as stiffness decreases. On the other hand, the highest and the lowest values of spectral acceleration (S_a) peak

in the response amplification range were obtained for Sat_15 (0.41g) and Dry (0.32 g), respectively.

A negligible influence of higher modes on FRS shape is observed, as a single spectral acceleration peak is obtained at the fundamental period, which ranges from 0.125 s for the Dry configuration to 0.167 s for Sat_15. On the other hand, closely-spaced modes effect could occur in this case, particularly referring to Figure 8a. In fact, the second mode period in Y direction of the Dry configuration is equal to 0.105 s.

The maximum value of the response amplification factor, *F*, was obtained at Floor 6 for all considered configurations. This unexpected peak at an intermediate level suggests local dynamic amplifications, which may not be captured by a first-mode approximation. This outcome is likely related to a minor higher-mode effect, as suggested by the irregularity of the structure in elevation. Such statement is confirmed by the participating mass ratios associated with the first translational modes, which result lower than 75% for all considered configurations. On the other hand, similar values of *F* were obtained at all floors, as reported in Table 6.

Configuration	*F*							
	Floor 1	Floor 2	Floor 3	Floor 4	Floor 5	Floor 6	Floor 7	Floor 8
Dry	3.965	4.225	3.841	4.010	4.008	**4.316**	4.047	3.995
Sat_15	4.458	4.854	4.203	3.839	4.488	**4.944**	4.504	4.365
Sat_85	4.194	4.444	3.981	3.772	4.148	**4.476**	4.147	4.051
Sat_mean	3.994	4.253	3.852	3.769	4.057	**4.357**	4.114	4.041

Table 6: Response amplification factors obtained for each configuration.

Overall, the results clearly show that moisture-induced stiffness degradation affects not only the magnitude of the seismic response, but also its record-to-record variability and its vertical distribution within the structure. This result highlights the importance of accounting for saturation effects in the seismic response assessment of masonry buildings, particularly for those exposed to major environmental degradation over time.

6 CONCLUSIONS

This study investigated the impact of moisture-induced degradation on the seismic response of a historic masonry building. A simplified degradation model to evaluate mechanical performance decay of masonry walls was firstly developed, based on literature data and in-situ testing. The model was used to compute mechanical properties of masonry walls in the case study building at different saturation levels, also considering the variability of the results due to model uncertainties. Linear time history analyses were performed on the case study building, aimed at calculating peak floor acceleration profiles along the height and floor response spectra based on the degradation level of masonry. The results showed that increasing saturation levels cause a shift in the fundamental period, related to masonry compressive strength and elastic modulus reduction. For the specific case study, this phenomenon resulted in greater acceleration response in case of high saturation level compared to the results referred to the dry masonry. In fact, peak floor accelerations and spectral accelerations at resonant periods increased progressively with moisture content. Moreover, minor higher modes effect was also observed, as the maximum spectral amplification was obtained at intermediate floors rather than the top floor.

The results confirm that water-induced stiffness degradation affects both the magnitude and the distribution of seismic demand and, consequently, the acceleration response.

Future developments are required for a comprehensive assessment of the effect of degradation on the seismic response of complex masonry structures, such as the variation of the non-linear response depending on the masonry saturation, the spatial distribution of the moisture and the effect of degradation on local failure modes.

REFERENCES

[1] G. Menditto, *Fessurazioni nelle strutture – Rilievo, lettura, diagnosi: una visione degli eventi degradanti alla luce delle nuove NTC*, Dario Flaccovio Editore, 2016.

[2] E. Tomasoni, *Analisi, verifiche e consolidamento strutturale di archi e volte – Manuale per la valutazione della sicurezza e per la progettazione degli interventi*, Dario Flaccovio Editore, 2021 .

[3] ISCARSAH, Recommendations For The Analysis, Conservation And Structural Restoration Of Architectural Heritage - Guidelines. *XIV Assemblea Generale dell'ICOMOS*, Victoria Falls – Zimbabwe, 2003.

[4] ICOMOS-ISCS (International Scientific Committee for Stone), Illustrated glossary on stone deterioration patterns, Champigny/Marne, Francia, 2008.

[5] F. Cherblanc, J. Berthonneau, P. Bromblet e V. Huon, Influence of Water Content on the Mechanical Behaviour of Limestone: Role of the Clay Minerals Content, *Geological Society, London, Special Publications,* **429**(1), 145–163, 2016.

[6] S. Yasar, Long term wetting characteristics and saturation induced strength reduction of some igneous rocks, *Environmental Earth Sciences,* **79**(14), 353, 2020.

[7] M. J. Heap, J. I. Farquharson, A. R. L. Kushnir, Y. Lavallée, P. Baud, H. A. Gilg e T. Reuschlé, The influence of water on the strength of Neapolitan Yellow Tuff, the most widely used building stone in Naples (Italy), *Bulletin of Volcanology,* **80**(6), 51, 2018.

[8] Á. Rabat, R. Tomás e M. Cano, Evaluation of mechanical weakening of calcarenite building stones due to environmental relative humidity using the vapor equilibrium technique, *Environmental Earth Sciences,* **79**(4), 80, 2020.

[9] E. Vasanelli, D. Colangiuli, A. Calia, M. Sileo e M. A. Aiello, Ultrasonic pulse velocity for the evaluation of physical and mechanical properties of a highly porous building limestone, *Ultrasonics*, **60**, 33–40, 2015.

[10] A. K. Tomor, J. M. Nichols e Z. Orbán, Evaluation of the loss of uniaxial compressive strength of sandstone due to moisture, *International Journal of Architectural Heritage*, 2023.

[11] N. Sathiparan e U. Rumeshkumar, Effect of moisture condition on mechanical behavior of low strength brick masonry, *Journal of Building Engineering*, **17**, 23-31, 2018.

[12] E. Franzoni, C. Gentilini, G. Graziani e S. Bandini, Compressive behaviour of brick masonry triplets in wet and dry conditions, *Construction and Building Materials,* **82**, 45-52, 2015.

[13] Ministero delle Infrastrutture e dei Trasporti, *Norme tecniche per le costruzioni*, DM 17 gennaio 2018.

[14] V. Athanasiou, A. D. Zervaki, E. Papamichos, A. Giannakopoulos, The use of Knoop indentation for the assessment of the elastic properties of mortars and natural stones, *International Journal of Rock Mechanics and Mining Sciences*, **83**, 241-247, 2016.

[15] E. Vasanelli, F. Micelli, D. Colangiuli, A. Calia e M. A. Aiello, A non destructive testing method for masonry by using UPV and cross validation procedure, *Materials and Structures*, **53**(134), 1-14, 2020.

[16] M. Petracca, F. Candeloro, G. Camata, STKO user manual. *ASDEA Software Technology*, Pescara, Italy, 2017.

[17] J. W. Baker, Conditional Mean Spectrum: Tool for ground motion selection, *Journal of Structural Engineering*, **137**(3), 322-331, 2011.